International Journal of Fatigue 170 (2023) 107548

Contents lists available at ScienceDirect

International Journal of Fatigue

journal homepage: www.elsevier.com/locate/ijfatigue

Energy-based critical plane fatigue methods applied to additively manufactured 18Ni300 steel

A.S. Cruces [a,*], R. Branco [b], L.P. Borrego [b,c], P. Lopez-Crespo [a,*]

[a] Department of Civil and Materials Engineering, University of Malaga, C/ Dr Ortiz Ramos s/n 29071 Malaga, Spain
[b] CEMMPRE, Department of Mechanical Engineering, University of Coimbra, 3030-788 Coimbra, Portugal
[c] Department of Mechanical Engineering, Coimbra Polytechnic - ISEC, Rua Pedro Nunes, 3030-199 Coimbra, Portugal

ARTICLE INFO

Keywords:
Biaxial fatigue
Mean stress
18Ni300 maraging steel
18Ni300 AM
Critical plane methods

ABSTRACT

In this work, the uniaxial and biaxial fatigue behaviour of maraging steel (18Ni300) obtained by additive manufacturing was studied. The material was evaluated using several biaxial load paths and different load levels. The predictive capacity of the fatigue life and crack initiation angle of the critical plane methods of Liu (I and II), and Chu, Conle, and Bonnen (CCB) were evaluated. The results obtained showed that normal stresses had a strong effect on the fatigue life. In general, the best estimates of the useful life and initial crack angle prediction were obtained with the CCB method.

1. Introduction

Fatigue behaviour of maraging steel produced by laser powder bed fusion is still not well understood, particularly in geometries containing geometric stress concentrations or experiencing multiaxial loading. The additive manufacturing technique presents some advantages that have not gone unnoticed in industry, especially in biomedical and aeronautic sectors [1]. Among the additive manufacturing (AM) techniques used to produce metal components of high quality, laser powder bed fusion has received increasing attention, because of its inherent advantages, such as good repeatability, medium productivity, and reasonable surface quality [2]. This method of manufacturing, based on fusing layers of metal powder particles [3], allows the production of pieces with complex designs, as well as optimisation of the use of the material. As in any manufacturing process, the microstructure and properties of the material will be affected to a greater or lesser extent by said process [4]. The drawbacks of the materials obtained using the aforementioned technique are related to their resistance. This is because a large number of defects are generated as a result of residual stresses or microstructural changes [5,6]. These defects will strongly affect the fatigue life of these materials, especially at high cycle numbers when crack nucleation periods dominate the process [7,8].

Maraging steel is a special class of engineering alloys which combines unusual properties, such as high strength and high toughness, along with weldability and dimensional stability. Its microstructure comprises a cubic martensitic matrix hardened by nanometer-size precipitates of intermetallic compounds formed from a metallurgical reaction that does not involve carbon promoting strengthening by precipitation hardening processes [9]. Due to its martensitic matrix, a fast quench from the austenitic region to temperatures below the martensite start temperature is required, which makes maraging steel especially suitable for laser powder bed fusion technology [9]. This success is generally explained by the small size of the melt pool which introduces very high cooling rates, but also by the cyclic reheating that occurs during the layer deposition which is associated with the nucleation of hardening precipitates without additional heat treatments. Nevertheless, this technique is prone to the occurrence of random defects distributed throughout the processed part, increasing the uncertainty associated with the mechanical behaviour [9].

Because fatigue resistance is key in most mechanical applications, numerous studies have been conducted on different materials to evaluate the effects of these defects on the resistance of the material. For example, Santos et al. investigated how the manufacturing speed affects the defect sizes and their relationship with fatigue resistance in 18Ni300 maraging steel, observing a decrease in resistance as the manufacturing speed increased [10]. Croccolo et al. studied the non-uniform distribution of defects caused by manufacturing direction and determined the importance of thermal and mechanical surface treatments to reduce the size and number of defects and their effects on strength [11,12]. Among these treatments, it is worth mentioning hot isostatic pressing, which

* Corresponding authors.
E-mail addresses: ascruces@uma.es (A.S. Cruces), plopezcrespo@uma.es (P. Lopez-Crespo).

https://doi.org/10.1016/j.ijfatigue.2023.107548
Received 30 October 2022; Received in revised form 25 January 2023; Accepted 26 January 2023
Available online 30 January 2023

achieves a significant improvement in mechanical behaviour [13]. Moreover, this improvement seems to have a noticeable effect when accompanied by a previous superficial mechanical treatment, given that, as observed by Molaei et al. [14], the high level of roughness that appears on the surface of the constructed pieces acts as a dominant factor in the fatigue resistance of the material.

The loading history also has an important role in fatigue strength. Regarding additively-manufactured materials, understanding its effect is even more challenging. Nevertheless, so far, most research has focused mainly on uniaxial loading conditions. Santos et al. [10] assessed the fatigue behaviour of 18Ni300 steel processed by laser powder bed fusion subjected to displacement-control and load-control modes. The stress-life relationships were significantly different for higher lives but relatively similar for lower lives. In the former case, the fatigue durability increased continuously with the decrease of the stress amplitude, when compared to the latter case, reaching a difference of more than 30 % for a service life of half a million cycles. Branco et al. [15] compared the fatigue behaviour of AM 18Ni300 steel under constant-amplitude and variable-amplitude loading. Fatigue life was reasonably predicted by combining the SWT parameter and a linear damage accumulation rule. Santos et al. [16] examined the effect of overloads on fatigue crack growth of 18Ni300 steel processed by laser powder bed fusion with and without post-processing heat treatments. Post-processing heat treatments effectively reduced the crack growth retardation after overload application.

A good understanding of the main fatigue damage mechanisms of this material, particularly under multiaxial loading, will help researchers to choose the most appropriate failure criteria in each case [13,17]. The various methods for estimating the fatigue life spans that exist include the critical plane methods. Since the inception of the additive manufacturing technique, different methods have been appearing to try to approximate, as best as possible, the fatigue behaviour of materials under multiaxial loads [18]. These methods are based upon observing the crack initiation and crack growth planes under different stress states [19]. Depending on the crack growth mode that governs the fatigue process, one critical plane method or another will be more appropriate [20]. Critical plane methods such as the Fatemi–Socie method correlate well with some additive manufacturing materials with a ductile behaviour [6,21]. Indeed, Branco et al. applied these methods in the same way for 18Ni300 maraging steel to obtain fatigue life estimates and predict the crack initiation angle under bending-torsion [22]. Cruces et al. [23] studied the notch effect on crack orientation and fatigue life under tension–torsion. Thus, more systematic research is needed to better understand the failure modes and the damage mechanisms associated with this alloy when subjected to multiaxial loading.

In this research, we studied the fatigue behaviour of additively manufactured 18Ni300 in the as-built condition. Thus, simple stress states such as uniaxial loading and pure torsion with complete inversion and biaxial-type stresses with in-phase tension–torsion, with and without applied mean stress, were applied. To cover the response of the material to different levels of fatigue lives, tests were carried out at three load levels for each load path. Finally, the study was completed by evaluating the energy-type critical plane methods from Liu I and II and Chu, Conle, and Bonnen (CCB).

2. Materials and methods

In this work, 18Ni300 maraging steel was studied. This material is an excellent candidate for additive manufacturing given its good toughness, strength, ductility, weldability and dimensional stability, thus being ideal for the different prostheses in the biomedical industry and components in the aerospace industry.

Table 1 summarises the monotonic properties of 18Ni300 maraging steel under study and Table 2 shows the uniaxial and torsional cyclic fatigue properties [24]. Load control mode was used during the experiments on MTS 809 servo-hydraulic rig, applying the loads through

Table 1
Monotonic properties of 18Ni300 steel.

Property	Value
Tensile strength, σ_u	925 MPa
Yield strength, σ_y	865 MPa
Young's Modulus, E	148 GPa

Table 2
Cyclic properties of 18Ni300.

Property	Value
Fatigue strength coefficient, σ'_f	1,798.73 MPa
Fatigue strength exponent, b	−0.1311
Fatigue ductility coefficient, ε'_f	0.32784
Fatigue ductility exponent, c	−1.0941
Fatigue shear strength coefficient, τ'_f	890.9 MPa
Fatigue shear strength exponent, b_γ	−0.103
Fatigue shear ductility coefficient, γ'_f	0.7806
Fatigue shear ductility exponent, c_γ	−0.899

sinusoidal curves. A biaxial extensometer (model Epsilon 3550) was used to measure the strains. In order to keep the extensometer in place, a 0.5 Hz frequency was used, so as to avoid sliding between the extensometer and the specimen. For the tests without mean stress (in which the ratchetting effect does not appear) the extensometer was disassembled at 2,000 cycles in cases in which the hysteresis loop had stabilised. For medium stress load paths, the extensometer was left on for the entire test. The test frequency was increased to 3 Hz after removing the extensometer. The end of test was set when a 2 % drop in the stabilised values of rotation or displacement was detected [25,26].

The specimen geometry used in this study is shown in Fig. 1. The building main axis in the fabrication of the specimens coincided with the tensile load direction of the specimen (horizontal direction in Fig. 1). Laser powder bed fusion was used to additively manufacture the specimens, using a Renishaw AM400 3D printer, with 400 W maximum power, 800 mm/s scan speed and 40 μm layer thickness throughout. No post-processing thermal or mechanical treatment was applied to the specimens, hence being tested in the as-built condition. The average surface roughness and maximum roughness amplitude values were 17.97 μm and 105.36 μm respectively. These were measured with a Mitutoyo surface roughness meter, model Surftest SJ-210.

The coordinate system considered in the work is shown in Fig. 2 and it is as follows: axial direction to the test piece - Z, radial - R, and peripheral - θ. The stress and strain values were obtained at the surface in the gauge part of the specimen, as shown in Fig. 2. The plane φ was defined by the angles α and β of the vector perpendicular to plane $\vec{n}$. The angle α was formed by the projection of $\vec{n}$ in the θR plane with the R axis. The angle β was formed by the vector $\vec{n}$ with the axial axis Z. To define the range of shear strains and stresses, we applied the Papadopoulos circumscribed circle theory [27].

Fig. 3 shows the load paths studied: uniaxial load with full reversal, pure torsion with full reversal, uniaxial load and torsion in phase, and full reversal torsion combined in phase with tensile load with 0.1 load ratio (R). The ratio of shear stress amplitude to normal stress amplitude for the biaxial load paths was $\lambda = 1.28$. Three different levels of equivalent stress amplitude were applied for the load paths, considering an equivalent stress amplitude ($\sigma_{a,eq}$) calculated using equation (1):

$$\sigma_{a,eq} = \sqrt{\sigma_a + 3\tau_a} \tag{1}$$

where σ_a is the stress ampltide, and τ_a is the shear stress amplitude. Table 3 summarises the different tests conducted in this work. First column shows the identification used for each specimen. The following columns include the equivalent stress amplitude ($\sigma_{a,eq}$), equivalent stress range ($\Delta\sigma$), mean stress (σ_m), shear stress range ($\Delta\tau$), axial strain range ($\Delta\varepsilon$), shear strain range ($\Delta\gamma$), fatigue life (N_f), and surface crack

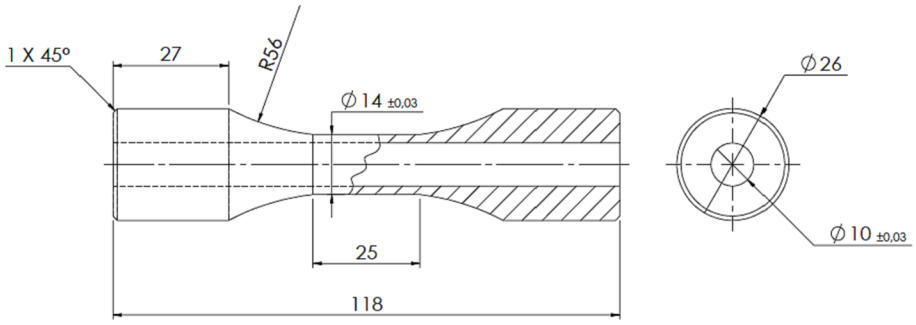

Fig. 1. Schematic of dog-bone shaped hollow specimens. The dimensions are given in mm.

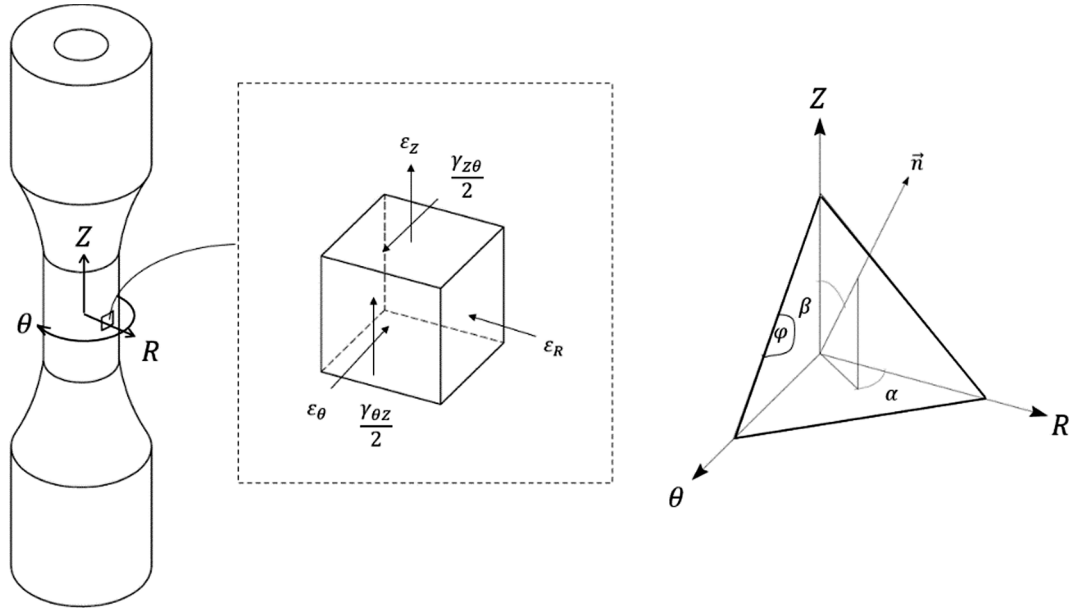

Fig. 2. Coordinate adopted in this work (a) and critical plane angles nomenclature (b).

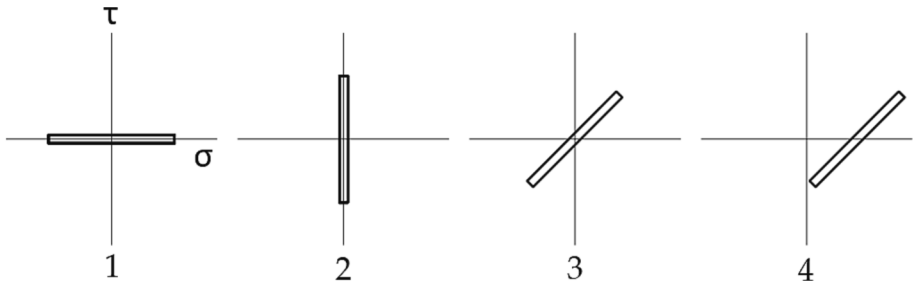

Fig. 3. Load paths used in the tests.

orientation ψ. The crack orientation was measured with Image-J software [28].

Fig. 4 plots the equivalent stress amplitude against the fatigue life for the four load paths studied. The stress amplitude was plotted against the fatigue life to highlight the changing effect of normal and torsional stress from the different load paths. Uniaxial and biaxial load paths with mean stress generated the greatest damage to the material. In both cases, the lives for each level of charge applied were similar. However, the pure torsion load path generated less damage because the plane of maximal shear strain was only subjected to shear stresses, (mode II), unlike the uniaxial case was under a combination of mode I and II stresses [17]. Finally, the biaxial load case without mean stress showed an intermediate fatigue life result. The stress state was the highest for the biaxial load path with mean stresses and the applied normal stress tended to open the crack, thereby reducing the fatigue life of the material [29].

After the test was completed, the specimen was roughened, first with number 240 sandpaper and then it was polished with number 800 paper to visualise the crack (Fig. 5). Next, the specimen was broken to analyse the fracture surface. Together with the measured crack angle at the surface, ψ, a general idea of the crack propagation through the material could also be obtained.

In most of the tests, the crack had propagated horizontally, with this result corresponding to propagation through defects oriented in the

Table 3
Summary of test conditions for the 12 specimens studied.

Id.	$\sigma_{a,eq}$ (MPa)	$\Delta\sigma$ (MPa)	σ_m (MPa)	$\Delta\tau$ (MPa)	$\Delta\varepsilon$ (%)	$\Delta\gamma$ (%)	N_f (cycles)	Crack angle ψ (°)
1A	385	767	0	0	0.56	0	22,427	0
1B	480	960	0	0	0.75	0	3784	0
1C	575	1151	0	0	0.91	0	1532	0
2A	385	0	0	443	0.04	0.815	259,535	42.73
2B	480	0	0	553	0.04	1.028	64,922	90
2C	575	0	0	664	0.06	1.302	7785	0
3A	385	315	0	404	0.29	0.813	54,793	0
3B	480	393	0	505	0.33	0.925	38,266	0
3C	575	472	0	606	0.41	1.194	10,273	0
4A	385	315	192.50	404	0.28	0.704	18,690	0
4B	480	393	240.50	505	0.34	0.955	4681	0
4C	575	472	288.75	606	0.93	1.161	1434	0

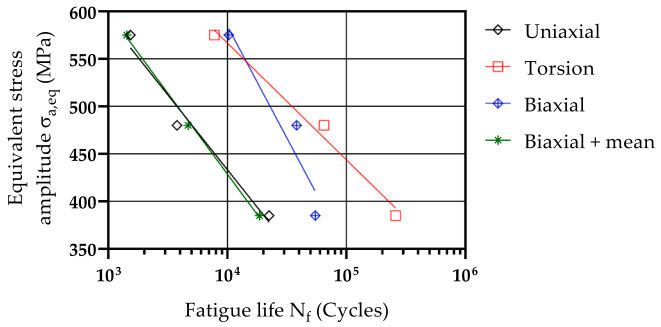

Fig. 4. Evolution of equivalent stress amplitude against fatigue life for each load path studied.

manufacturing planes of the specimen [13]. For the uniaxial load path, in every case, the surface crack angles were equal and were approximately 0° with respect to the horizontal. For the lower load test, a main crack covering the entire thickness was observed. In the pure torsion load path for the smallest load level (A), it was impossible to determine the crack initiation zone. However, a growth plane approximately 42.73° with respect to the horizontal was observed. For load levels B and C, the crack grew vertically and horizontally, respectively, coinciding with the plane of maximal shear stresses (Fig. 5). Similar results were obtained in tests with pure torsion in M250 maraging steel in which initial crack growth was observed preferentially in mode II [30].

Fig. 6 shows an image of the specimen with a biaxial load with mean stress (4A) in which the estimated crack initiation point is indicated with a red arrow. The crack began to grow in a horizontal plane not coinciding with the plane of maximum range of shear strain $\Delta\gamma_{max}$ or with that of maximum normal deformation $\Delta\varepsilon_{max}$, which form 15° and 30° angles, respectively, with respect to the horizontal (Fig. 6). In any case, growth was initially close to the maximum shear strain values. Once the crack reached a certain length, it was rotated to line up in the directions of maximum normal strain. As shown in Fig. 6b, no indication of this change in the crack growth mode was apparent from the surface examination. For the relationship between applied shear and normal stresses, some materials tend to show a similar behaviour, which is dominated by mode II cracks [31].

3. Fatigue life prediction models

Critical plane methods were developed based upon observing cracks nucleating and growing on specific planes. The orientation of such planes is used to define the dominant planes in which a damage parameter representative of material failure under different stress states is obtained. In this way, critical plane methods are capable of predicting both the fatigue life and the initial crack propagation angle [32].

The methods studied in this work, Liu I, Liu II, and CCB, are based on strain energy concepts. This type of energy-based approach attempts to make more physical sense of critical plane methods [33]. To identify the critical plane in the different methods, a scan of the stresses that appear in different planes with respect to the reference plane was performed with increments of 5° for each angle α and β that define the critical plane according to the coordinate system shown in Fig. 2.

3.1. Liu I and Liu II

The methods defined by Liu [16] are based on strain energy in the cycle. In this approach, the different behaviour of the materials in relation to the growth of the crack were considered. Thus, the method

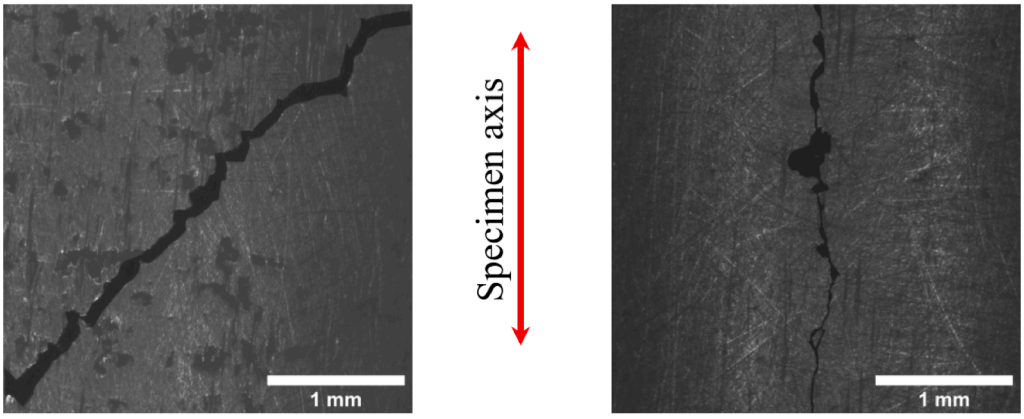

Fig. 5. Crack angles for pure torsion load path 2A and 2B.

(a) (b) (c)

Fig. 6. Failure surface of the tested sample 4A – Biaxial with mean stress.

considers cases in which the crack growth was dominated by mode I or mode II growth, defining a method in which the plane in which the normal strain energy (equation (2)) or shear strain energy (equation (3)) was maximised, respectively. The damage parameter included the elastic and plastic deformation energy in order to correctly consider fatigue damage and thus, failure due to fatigue was considered at high cycles in which the plastic deformation component would be almost negligible. The Liu I (Eq. (2)) and Liu II (Eq. (3)) damage parameters were modified to take the effect of mean stresses into account as follows:

$$\left[(\Delta\sigma_n\Delta\varepsilon_n)_{max}+(\Delta\tau\Delta\gamma)\right]\left(\frac{2}{1-R}\right)=4\sigma_f'\varepsilon_f'(2N_f)^{b+c}+\frac{4\sigma_f'^2}{E}(2N_f)^{2b} \quad (2)$$

where $\Delta\sigma_n$ is the range of normal stress, $\Delta\varepsilon_n$ is the range of normal strain, $\Delta\tau$ is the range of shear stress, $\Delta\gamma$ is the range of shear strain, R is the load ratio, ε'_f is the fatigue ductility coefficient, σ'_f is the fatigue strength coefficient, b is the fatigue strength exponent, c is the fatigue ductility exponent, and E is the Young's modulus.

$$\left[(\Delta\sigma_n\Delta\varepsilon_n)+(\Delta\tau\Delta\gamma)_{max}\right]\left(\frac{\sigma'_f}{\sigma'_f-\sigma_{n,mean}}\right)=4\tau_f'\gamma_f'(2N_f)^{b\gamma+c\gamma}+\frac{4\tau_f'^2}{G}(2N_f)^{2b\gamma} \quad (3)$$

where $\sigma_{n,mean}$ is the mean normal stress, τ'_f is the shear strength coefficient in fatigue, b_γ is the shear strength exponent in fatigue, γ'_f is the shear ductility coefficient in fatigue, c_γ is the shear ductility exponent in fatigue, and G is the shear modulus.

3.2. Chu, Conle, and Bonnen

Chu et al. [34] define an energy-type damage parameter by combining the axial and shear effect (equation (4)). Unlike the Liu's methods, the normal and shear stress ranges are replaced by the maximal values in the critical plane. This change makes it possible to include the effect of the average stresses in the damage parameter. The plane that maximises ΔW is used to define the critical plane. When considering the maximum value, the parameter does not distinguish a priori between the dominance of one crack growth mode or another, but rather, based on the applied load conditions.

$$\Delta W=\tau_{n,max}\frac{\Delta\gamma}{2}+\sigma_{n,max}\frac{\Delta\varepsilon}{2} \quad (4)$$

The resistance curve for the damage parameter is obtained from the uniaxial cyclic curve of the material [17]. The uniaxial curve is modified to consider the plane maximising the damage parameter defined in equation (4). Because the weight of the elastic and plastic part varies with cycles, the critical plane also varies slightly for the same uniaxial load case. In the resistance curve, the coefficients that multiply the elastic and plastic parts are defined in the planes that maximise the damage parameter at low cycles when the weighting of the plastic part is greatest and at high cycles when the elastic part has the greatest weighting.

$$\Delta W=1.02\frac{\sigma'^2_f}{E}(2N_f)^{2b}+1.041\sigma'_f\varepsilon'_f(2N_f)^{b+c} \quad (5)$$

The predictive capability of the methods was statistically studied with the mean and the error deviation between the experimental value and the one returned by the method. For the fatigue life, the error was considered equal to the difference between the experimental value and that of the method on a logarithmic scale [35], see equation (6).

$$error_{Nf}=\log_{10}(N_{th})-\log_{10}(N_{exp}) \quad (6)$$

4. Results and analysis

The fatigue life estimations for Liu I (a), Liu II (b), and CCB (c) methods are shown in Fig. 7. The results are presented on a logarithmic scale with bands of results deviation by ± 2 with respect to the theoretical life span.

Starting with the two Liu methods, more cohesive results were observed for the biaxial cases with Liu I. Greater weighting was applied to the normal deformation energy part of the equation to try to achieve a better approximation to the behaviour of the material (by considering it less ductile or with a fatigue failure dominated by growth in mode I). Previous tests conducted by Branco et al. on 18Ni300 with in-phase biaxial loads [22] support the results obtained here. In torsion, Liu I returns very few conservative values for the three load levels compared to Liu II, although the latter provides more conservative values within ± 2 deviation bands with respect to the theoretical life span. For these cases, the initiation and growth of the crack are close to those of planes with $\Delta\gamma_{max}$ (Table 3), thereby suggesting a failure in which mode II dominates and for which the Liu I method does not define damage representative of the failure. In the uniaxial case, the result returned by each Liu method was opposite to that of pure torsion, but with a greater deviation towards more conservative results at higher cycles in the case of Liu II. In the biaxial in-phase case, the results were more accurate and less conservative with Liu I than with Liu II. The opposite result was observed in the method predictions for the same type of load path in a previous study with an S355 steel [36]. For the case of biaxial stresses with mean stress levels, the results with Liu I were more conservative than with Liu II. This result was probably caused by the stress being applied for the same range of normal and shear stresses as that applied without mean stress causing torsional deformations equal to or slightly lower than those shown in Table 3. In turn, a clear increase in values was observed for higher load levels in the axial strain part. In all the tests, more conservative results were obtained by the CCB method than with the Liu methods. Thus, defining the damage parameter in the plane in which it is maximal and including the normal and shear strain parts

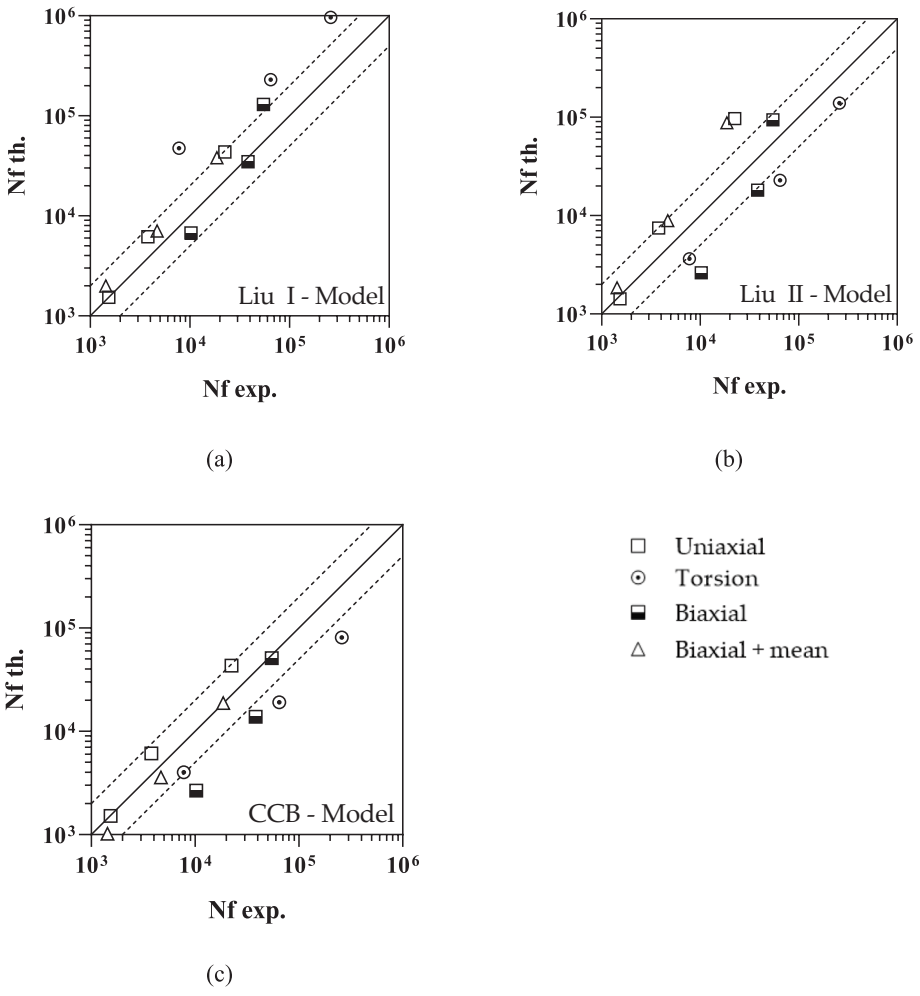

Fig. 7. Fatigue life estimation on AM 18Ni300 steel based of Liu I, Liu II and CCB methods against the experimental life.

seems to respond better to the change in material behaviour as a function of the applied stress state.

The mean values and standard deviations of the error are shown in Table 4. Values are calculated according to equation (6), for the fatigue life estimates of the methods. On the one hand, based on the performance of the three methods, Liu I produced the lowest deviations in the results. However, it did not seem to respond well to tests with torsional loads. On the other hand, the CCB method produced results with a slightly higher deviation compared to Liu I, but with more conservative results. In general, it can be considered more appropriate because it is more cautious when estimating fatigue lives for materials.

The experimental surface crack angles versus those estimated by each method are shown in Table 5. The angle ψ of the methods was calculated as the angle with respect to the horizontal of the crossing line between critical plane and θZ plane (see Fig. 2). Angles shown in Table 5 are those corresponding to the critical plane closest to the experimental one for cases in which the parameter defined by the method was maximal in two different planes. In uniaxial-type tests, the difference between the methods would appear in the angle of the plane in the radial direction for which no experimental measurements have yet been made.

Table 4
Summary of statistical values of the different methods.

Variables	Liu I	Liu II	CCB
Mean value	0.2653	0.0185	−0.1797
Standard deviation	0.2778	0.4184	0.2912

For biaxial-type tests, the CCB method would be closer to the experimental method than Liu II and so we consider that CCB defined the critical plane more precisely than the Liu I and II methods did. The fatigue life of sample 2A was considerably larger than that of the other specimens (see Table 3), with it being in the high cycle regime [37] unlike the rest of samples. This difference with respect the rest of samples is probably the determining factor to induce a different orientation. Indeed, materials subjected to pure torsion on the high cycle fatigue regime tend to show a mode I dominated cracking [21,38].

The large differences in cracking angle during torsion are probably due to the load level. Depending on the microstructure, the stress state and whether the crack is under LCF or HCF, the length of crack initiation and crack propagation change. Torsion stress tends to produce maximum shear strain planes at 0° and 90° with respect the specimen axis. High load levels induce growth on planes with maximum shear and micro-cracks often initiate at multiple points because there exists enough energy for their growth and subsequent coalescence of micro-cracks into a macro-crack. Lower loads produce smaller number of points from which crack propagate, because there is less energy available for this purpose and only most critical locations will extend. Moreover, for additively manufactured materials, the defect density is often higher in the direction normal to manufacturing direction [13]. The manufacturing direction in this work was the axial direction (depicted in Fig. 5) thus inducing a higher defect density on planes perpendicular to this direction. This is observed in sample 2C. Conversely, sample 2B shows the opposite behaviour (90° instead of 0°). Previous studies observed such 90° orientation for supposedly pure

Table 5
Comparison of surface crack angle ψ measured with studied methods predictions.

	1A	1B	1C	2A	2B	2C	3A	3B	3C	4A	4B	4C
Experimental	0	0	0	42.73	90	0	0	0	0	0	0	0
Liu I	0	0	0	45	45	45	30	30	30	30	30	30
Liu II	0	0	0	90/0	90/0	90/0	15	15	15	15	15	15
CCB	0	0	0	90/0	90/0	90/0	5	5	5	10	10	10

torsion tests where a small axial compressive component appeared [39]. Even though the experiment could be designed for pure torsional loads, experimental misalignments might induce slight compressive loads. Accordingly, the load registry was carefully checked to identify possible compressive loads. No compressive load was detected throughout the test. An alternative reasoning for the behaviour observed on 2B is the existence of an abnormally large defect in the longitudinal direction.

5. Conclusions and prospective work

This work allowed the fatigue response of additively manufactured 18Ni300 steel to be evaluated through uniaxial, torsion, and biaxial tests, with and without mean stress. Based on the results obtained, the main conclusions are as follows:

1. The normal stresses applied to slip planes strongly affect the material. This is linked to the higher defect density along the planes normal to the axial direction.
2. The initial crack growth angles were measured at the surface of the specimen. For the biaxial load paths on the surface of the specimen, a crack was observed that followed the plane of maximal shear strain until failure, but after analysing the fracture surface, we saw that the crack orientated towards the plane of maximal normal strain when it reached a certain length.
3. Three critical plane methods based on strain energy, Liu I, Liu II, and CCB, were also applied. The three methods were comparable in terms of their fatigue life predictions. Liu I showed the best results for uniaxial tensile cases and biaxial cases on the AM 18Ni300 steel under study, in agreement with a previous analysis. This suggests that AM 18Ni300 steel fails predominantly under brittle fracture behaviour. Uniaxial loads modify the behaviour inducing a more brittle mode.
4. The CCB method produced better results in the uniaxial and torsional cases because it showed greater flexibility in the damage parameter when considering the behaviour of this material (such as its brittleness or ductility) with other stress states applied. In every case, the results returned by the CCB method were more conservative than those obtained with the Liu methods. Considering its low deviation from the fatigue life estimates and that it was more conservative, the CCB method returned the best results for the material for the load paths studied. CCB also provided better estimates of the initial crack growth plane for all the tests conducted, except for the torsional load path with the lowest load level.

Because of the triangular dependency between process parameters, microstructure and mechanical properties is rather complex for AM materials, additional research is being conducted to extend the current knowledge on multiaxial fatigue behaviour of SLM 18Ni300, namely: (1) the analysis of other loading cases, including out-of-phase loading; (2) the effect of different post-processing treatments on porosity levels, microstructure, damage mechanisms, and fatigue life; and (3) the development of a tuned multiaxial fatigue life model for this AM alloy.

Declaration of Competing Interest

The authors declare that they have no known competing financial interests or personal relationships that could have appeared to influence the work reported in this paper.

Data availability

Data will be made available on request.

Acknowledgements

Authors would like to acknowledge the following financial support: FEDER Programa Operativo by Junta de Andalucia (Spain) - grant reference UMA18-FEDERJA-250; COMPETE2020 Program from European Funds, under Eureka Smart label S0129-AddDies (Grant reference POCI-01-0247-FEDER-042536) and funds by the Portuguese Fundação para a Ciência e a Tecnologia with Grant UIDB/00285/2020 and Grant LA/P/0112/2020. We would also like to acknowledge funding for open access charge: Universidad de Malaga / CBUA. Authors would also like to acknowledge industrial support from Dr. Alfonso Garcia-Priego (Prosthetic Unit), Mr. Alfonso Exposito, Ubeda San Juan de la Cruz Hospital (Jaen, Spain) and the High Resolution Cazorla Hospital (Jaen, Spain).

References

[1] Gorelik M. Additive manufacturing in the context of structural integrity. Int J Fatigue 2017;94:168–77.
[2] Sefene EM. State-of-the-art of selective laser melting process: a comprehensive review. J Manuf Syst 2022;63:250–74.
[3] Yadroitsev I, Bertrand P, Smurov I. Parametric analysis of the selective laser melting process. Appl Surf Sci 2007;253:8064–9.
[4] Pegues JW, Shao S, Shamsaei N, Sanaei N, Fatemi A, Warner DH, et al. Fatigue of additive manufactured Ti-6Al-4V, Part I: The effects of powder feedstock, manufacturing, and post-process conditions on the resulting microstructure and defects. Int J Fatigue 2020;132.
[5] Fayazfar H, Salarian M, Rogalsky A, Sarker D, Russo P, Paserin V, et al. A critical review of powder-based additive manufacturing of ferrous alloys: process parameters, microstructure and mechanical properties. Mater Des 2018;144:98–128.
[6] Molaei R, Fatemi A, Phan N. Notched fatigue of additive manufactured metals under axial and multiaxial loadings, Part I: effects of surface roughness and HIP and comparisons with their wrought alloys. Int J Fatigue 2021;143:106003.
[7] Murakami Y, Endo T. Effects of small defects on fatigue strength of metals. Int J Fatigue 1980;2:23–30.
[8] Meneghetti G, Rigon D, Gennari C. An analysis of defects influence on axial fatigue strength of maraging steel specimens produced by additive manufacturing. Int J Fatigue 2019;118:54–64.
[9] Tan C, Zhou K, Ma W, Zhang P, Liu M, Kuang T. Microstructural evolution, nanoprecipitation behavior and mechanical properties of selective laser melted high-performance grade 300 maraging steel. Mater Des 2017;134:23–34.
[10] Santos LMS, Ferreira JAM, Jesus JS, Costa JM, Capela C. Fatigue behaviour of selective laser melting steel components. Theor Appl Fract Mech 2016;85:9–15.
[11] Croccolo D, De Agostinis M, Fini S, Olmi G, Vranic A, Ciric-Kostic S. Influence of the build orientation on the fatigue strength of EOS maraging steel produced by additive metal machine. Fatigue Fract Eng Mater Struct 2016;39:637–47.
[12] Croccolo D, Agostinis M, Fini S, Olmi G, Robusto F, Ciric-Kostic S, et al. Sensitivity of direct metal laser sintering Maraging steel fatigue strength to build orientation and allowance for machining. Fatigue Fract Eng Mater Struct 2018;42.
[13] Yadollahi A, Shamsaei N. Additive manufacturing of fatigue resistant materials: challenges and opportunities. Int J Fatigue 2017;98:14–31.
[14] Molaei R, Fatemi A, Phan N. Significance of hot isostatic pressing (HIP) on multiaxial deformation and fatigue behaviors of additive manufactured Ti-6Al-4V including build orientation and surface roughness effects. Int J Fatigue 2018;117:352–70.
[15] Branco R, Silva J, Ferreira JM, Costa JD, Capela C, Berto F, et al. V Fatigue behaviour of maraging steel samples produced by SLM under constant and variable amplitude loading. Procedia Struct Integr 2019;22:10–6.
[16] Santos LMS, Borrego LP, Ferreira JAM, de Jesus J, Costa JD, Capela C. Effect of heat treatment on the fatigue crack growth behaviour in additive manufactured AISI 18Ni300 steel. Theor Appl Fract Mech 2019;102:10–5.

[17] Socie DF, Marquis GB. Multiaxial fatigue, 1st ed. Warrendale, PA (USA): Society of Automotive Engineers, Inc.; 2000.
[18] Karolczuk A, Macha E. A review of critical plane orientations in multiaxial fatigue failure criteria of metallic materials. Int J Fract 2005;134:267–304.
[19] Brown MW, Miller KJ. A theory for fatigue failure under multiaxial stress-strain conditions. Proc Inst Mech Eng 1973;187:745–55.
[20] Socie D. Multiaxial fatigue damage models. J Eng Mater Technol 1987;109:293–8.
[21] Fatemi A, Molaei R, Phan N. Multiaxial fatigue of additive manufactured metals: performance, analysis, and applications. Int J Fatigue 2020;134:105479.
[22] Branco R, Costa JD, Ferreira JAM, Capela C, Antunes FV, Macek W. Multiaxial fatigue behaviour of maraging steel produced by selective laser melting. Mater Des 2021;201:109469.
[23] Cruces AS, Exposito A, Branco R, Borrego LP, Antunes FV, Lopez-Crespo P. Study of the notch fatigue behaviour under biaxial conditions of maraging steel produced by selective laser melting. Theor Appl Fract Mech 2022;121:103469.
[24] Branco R, Costa JDM, Berto F, Mohammad S, Razavi J, Ferreira AM, et al. Low-cycle fatigue behaviour of AISI 18Ni300 maraging steel produced by selective laser melting. Metals (Basel) 2018.
[25] Shamsaei N, Gladskyi M, Panasovskyi K, Shukaev S, Fatemi A. Multiaxial fatigue of titanium including step loading and load path alteration and sequence effects. Int J Fatigue 2010;32:1862–74.
[26] Jen YM, Wang WW. Crack initiation life prediction for solid cylinders with transverse circular holes under in-phase and out-of-phase multiaxial loading. Int J Fatigue 2005;27:527–39.
[27] Papadopoulos I. A comparative study of multiaxial high-cycle fatigue criteria for metals. Int J Fatigue 1997;19:219–35.
[28] ImageJ. Available from: https://imagej.net/Welcome (accessed on Feb 22, 2019).
[29] Fatemi A, Socie DF. A critical plane approach to multiaxial fatigue damage including out-of-phase loading. Fatigue Fract Eng Mater Struct 1988;11:149–65.
[30] Pinna C, Doquet V. Preferred fatigue crack propagation mode in a M250 maraging steel loaded in shear. Fatigue Fract Eng Mater Struct 2001;22:173–83.
[31] Susmel L, Petrone N. Multiaxial fatigue life estimations for 6082-T6 cylindrical specimens under in-phase and out-of-phase biaxial loadings. In: Carpinteri A, de Freitas M, Spagnoli ABT-ESIS, editors. Biaxial/multiaxial fatigue and fracture. Vol. 31. Elsevier; 2003. p. 83–104. ISBN 1566-1369.
[32] Socie D. Multiaxial fatigue. *Multiaxial Fatigue* 1999, 113.
[33] Glinka G, Shen G, Plumtree A. A multiaxial fatigue strain energy parameter related to the critical plane. Fatigue Fract Eng Mater Struct 1995;18:37–46.
[34] Chu CC, Conle FA, Bonnen JJF. Multiaxial stress-strain modeling and fatigue life prediction of SAE axle shafts. Adv. Multiaxial Fatigue, ASTM STP 1191. 1993: 33–54.
[35] Erickson M, Kallmeyer AR, Van Stone RH, Kurath P. Development of a multiaxial fatigue damage model for high strength alloys using a critical plane methodology. J Eng Mater Technol 2008;130:041008 1–041008 9.
[36] Cruces AS, Lopez-Crespo P, Moreno B, Antunes FV. Multiaxial Fatigue Life Prediction on S355 Structural and Offshore Steel Using the SKS Critical Plane Model. 2018.
[37] Suresh S. Fatigue of materials, 2nd ed. Cambridge: Cambridge University press; 1998.
[38] Chaves V, Navarro A, Madrigal C. Stage I crack directions under in-phase axial–torsion fatigue loading for AISI 304L stainless steel. Int J Fatigue 2015;80: 10–21.
[39] Ngeru T, Kurtulan D, Karkar A, Hanke S. Mechanical behaviour and failure mode of high interstitially alloyed austenite under combined compression and cyclic torsion. Metals (Basel) 2022:12.